Interaction potential for SiO_2: A molecular-dynamics study of structural correlations

P. Vashishta, Rajiv K. Kalia, and José P. Rino*
Argonne National Laboratory, Argonne, Illinois 60439-4843

Ingvar Ebbsjö
The Studsvik Neutron Research Laboratory, S-611 82 Nyköping, Sweden
(Received 11 July 1989)

An interaction potential consisting of two-body and three-body covalent interactions is proposed for SiO_2. The interaction potential is used in molecular-dynamics studies of structural and dynamical correlations of crystalline, molten, and vitreous states under various conditions of densities and temperatures. The two-body contribution to the interaction potential consists of steric repulsion due to atomic sizes, Coulomb interactions resulting from charge transfer, and charge-dipole interaction to include the effects of large electronic polarizability of anions. The three-body covalent contributions include O-Si-O and Si-O-Si interactions which are angle dependent and functions of Si-O distance. In lattice-structure calculations with the total potential function, α-cristobalite and α-quartz are found to have the lowest and almost degenerate energies, in agreement with experiments. The energies for β-cristobalite, β-quartz, and keatite are found to be higher than those for α-cristobalite and α-quartz. Molecular-dynamics calculations with this potential function correctly describe the short- and intermediate-range order in molten and vitreous states. In the latter, partial pair-distribution functions give Si—O, O—O, and Si—Si bond lengths of 1.62, 2.65, and 3.05 Å, respectively. The vitreous state consists of nearly ideal $Si(O_{1/2})_4$ tetrahedra in corner-sharing configurations. The Si—O—Si bond-angle distribution has a peak at 142° and a full width at half maximum (FWHM) of 25° in good agreement with nuclear magnetic resonance experiments. The calculated static structure factor is also in agreement with neutron-diffraction experiments. Partial static structure factors reveal that intermediate-range Si-Si, O-O, and Si-O correlations between 4 and 8 Å give rise to the first sharp diffraction peak (FSDP). The FSDP is absent in charge-charge structure factor, which indicates that charge neutrality prevails over length scales between 4 and 8 Å. Dynamical correlations in vitreous and molten states, phonon densities of states of crystalline and vitreous SiO_2, infrared spectra of crystalline, vitreous and molten states, isotope effect, distribution of rings and their structure in molten and vitreous states, and structural transformations at high pressures will be discussed in subsequent papers.

I. INTRODUCTION

Silicon dioxide is one of the most extensively studied materials in condensed-matter physics, chemistry, materials science, and engineering.[1] Although crystalline SiO_2 is known to have as many as 40 different structures,[2,3] only cristobalite,[4] quartz,[3,5] coesite,[6] and stishovite[7] have a temperature-density field of thermodynamic stability for chemically pure SiO_2 (no other element added for structural stability). Structures of α- and β-cristobalites and quartz at atmospheric pressure, and coesite at high pressures, involve different arrangements of nearly ideal corner-sharing $Si(O_{1/2})_4$ tetrahedra.[2,8] However, the densest structure of SiO_2, namely stishovite, has distorted $Si(O_{1/3})_6$ octahedra sharing edges and corners.[2]

Table I lists the densities, crystal structures, bond lengths, and bond angles (O—Si—O and Si—O—Si) for β- and α-cristobalites, keatite,[3,8] β- and α-quartz, coesite, and stishovite. It is intriguing that β-cristobalite and coesite have the same Si—O bond length and O—Si—O bond angle even though their densities differ by 33%. On the other hand, this increase in the density increases the average Si—O—Si bond angle and also changes the connectivity of the tetrahedra. Additionally, the distribution of rings also changes from six in β-cristobalite to four, six, and eight in coesite.[2]

It is conceivable that the richness of crystalline forms of SiO_2 may even extend into the molten and vitreous states at different temperatures and pressures. The structures of the vitreous and molten states have been studied extensively with x-ray and neutron-diffraction techniques.[9–26] It should be remembered that unlike crystals the diffraction measurements in amorphous systems provide only an angle-averaged function of the magnitude of the wave vector $|\mathbf{q}|$. Structural correlations have also been inferred from nuclear magnetic resonance (NMR),[27,28] Raman,[15,29–32] and infrared[15,33,37] measurements. Structural transformations in a-SiO_2 under pressure have been investigated with neutron[34] and Brillouin scattering.[35,36]

Several different approaches have been used to understand the structure of a-SiO_2. The first approach, proposed by Lebedev[38] in 1921, states that the structure of a-SiO_2 consists of "microcrystallites," and in 1936 this

was extended by Valenkov and Porai-Koshits.[39] In 1932, Zachariasen[40] proposed the continuous-random-network model for a-SiO_2, which was extended by Warren, Krutter, and Morningstar[9] in 1936. In 1982, Phillips[41] proposed the "paracrystallite" model, based on the presence of ~66-Å-diam β-cristobalite crystallites.

Bell and Dean[42] have attempted to explain the structure and dynamics of a-SiO_2 using a ball-and-stick cluster model. Attempts have been made by Gaskell and Tarrant,[43] and Robertson and Moss[44] to relax the strain in the Bell-Dean model with a Keating-type[45] potential function. Structural correlations and the vibrational spectrum of a-SiO_2 have been investigated by Sen and Thorpe,[46] Thorpe and Galeener,[47] de Leeuw and Thorpe,[48] and Guttman and Rahman[49] using random-network models. Models of a-SiO_2 based on Bethe lattice have been used by Laughlin and Joannopoulos,[50] and Galeener *et al.*,[51] and Barrio *et al.*[52] In contrast to random-network models that have well-defined distribution of ring sizes, models based on Bethe lattice have no closed rings.

The first molecular-dynamics (MD) calculations for a glass (BeF_2) were performed by Rahman, Fowler, and Narten.[53] In 1976, Woodcock, Angel, and Cheeseman[54] carried out an MD simulation of a-SiO_2 using a purely ionic interaction consisting of Born-Mayer-Huggins repulsion and Coulomb interaction. Since then, several MD simulations have been performed with full ionic potentials or truncated Coulomb interaction. Soules[55] studied a-SiO_2 and silicate glasses; Mitra, Amin, Fincham,

TABLE I. Density, crystal structure, bond lengths, and bond angles for a few crystalline forms of SiO_2. Names of the structures are given in the first column. In the second column, the upper number denotes the mass density in g/cm^3, whereas the lower number in parentheses represents the number density in units of 10^{22} cm^{-3}. Group symmetry and number of SiO_2 molecules per unit cell (mol/u.c.) are given in the third column. In the fourth column the upper numbers give Si—O bond lengths and the lower numbers, $\langle$Si—O$\rangle$, represent the average bond length. In the last column values of bond angles Si—O—Si, average value $\langle$Si—O—Si$\rangle$, bond angle O—Si—O, and its average value $\langle$O—Si—O$\rangle$ are given.

Name	Mass and number densities g/cm^3 (10^{22} cm^{-3})	Crystal structure	Bond length (Å)	Bond angles (deg)
β-cristobalite[a]	2.20 (6.618)	cubic ($Fd3m$) 8 mol/u.c.	$d_{Si-O}=1.611$ $\langle d_{Si-O}\rangle=1.611$	$\sphericalangle$Si—O—Si = 146.7 $\langle\sphericalangle$Si—O—Si$\rangle$ = 146.7 $\sphericalangle$O—Si—O = 107.8,112.8
α-cristobalite[b]	2.35 (7.088)	tetragonal ($P4_12_1$) 4 mol/u.c.	$d_{Si-O}(1)=1.602$ $d_{Si-O}(2)=1.617$	$\sphericalangle$Si—O—Si = 144.7 $\langle\sphericalangle$Si—O—Si$\rangle$ = 144.7 $\sphericalangle$O—Si—O = 108.1–111.3 $\langle\sphericalangle$O—Si—O$\rangle$ = 109.5
keatite[c]	2.50 (7.526)	tetragonal ($P4_12$) 12 mol/u.c.	$d_{Si-O}=1.56$–1.62 $\langle d_{Si-O}\rangle=1.590$	$\sphericalangle$Si—O—Si = 148.2–159.5 $\langle\sphericalangle$Si—O—Si$\rangle$ = 155.2 $\sphericalangle$O—Si—O = 103.7–113.8
β-quartz[d]	2.52 (7.57)	hexagonal ($P6_22$) 3 mol/u.c.	$d_{Si-O}(1)=1.591$ $d_{Si-O}(2)=1.606$	$\sphericalangle$Si—O—Si = 150.9 $\langle\sphericalangle$Si—O—Si$\rangle$ = 150.9 $\sphericalangle$O—Si—O = 108.0–110.5
α-quartz[e]	2.65 (7.956)	trigonal ($P3_221$) 3 mol/u.c.	$d_{Si-O}(1)=1.605$ $d_{Si-O}(2)=1.614$ $\langle d_{Si-O}\rangle=1.609$	$\sphericalangle$Si—O—Si = 143.7 $\langle\sphericalangle$Si—O—Si$\rangle$ = 143.7 $\sphericalangle$O—Si—O = 108.7–110.4
coesite[f]	2.92 (8.784)	monoclinic ($P21/a$) 16 mol/u.c.	$d_{Si-O}=1.60$–1.62 $\langle d_{Si-O}\rangle=1.609$	$\sphericalangle$Si—O—Si = 137.4–180 $\langle\sphericalangle$Si—O—Si$\rangle$ = 148.4 $\sphericalangle$O—Si—O = 107.9–110.5 $\langle\sphericalangle$O—Si—O$\rangle$ = 109.5
stishovite[g]	4.29 (12.88)	tetragonal ($P4_2/mnm$) 2 mol/u.c.	$d_{Si-O}(1)=1.809$ $d_{Si-O}(2)=1.757$	$\sphericalangle$Si—O—Si = 81,90,106[h] $\sphericalangle$O—Si—O = 100,130

[a]References 3 and 8.
[b]Reference 4.
[c]References 3 and 8.
[d]References 3 and 8.
[e]Reference 5.
[f]Reference 6.
[g]Reference 7.
[h]We have calculated these angles using the structural parameters for stishovite given in Ref. 7.

and Hockney,[56] and Mitra[57] investigated the properties of a-SiO_2. Garofalini[58] performed MD calculations for a-SiO_2 and silicate glasses using truncated Coulomb interactions. Kubicki and Lasaga[59] have studied a-SiO_2 using a simple ionic model with Born-Mayer repulsion terms and central-force-field covalent potentials. Feuston and Garofalini[60] have used short-ranged two- and three-body interactions to investigate the properties of a-SiO_2.

In this paper, we investigate structural correlations in molten and a-SiO_2 using the proposed interaction potential with the MD method. The structural issues we have addressed include short-range order and intermediate-range correlations manifested in the form of the first sharp diffraction peak. This paper is divided into six sections. The interaction potential is discussed in Sec. II. In Sec. III we discuss the energies of the crystalline structures of SiO_2 based on our model of interaction potential. Details of MD simulations, the preparation of vitreous states, a discussion of correlation functions used in the analysis of MD results, and the comparison with experiments are given in Sec. IV. In Sec. V, results for short- and intermediate-range order are discussed; results for the molten state are also given. Concluding remarks are given in Sec. VI.

II. INTERACTION POTENTIAL

Monoatomic systems with close-packed structures can be reasonably well described by two-body interaction potentials. The essence of these potentials lies in the fact that the repulsive part describes the scale of atomic size and the attractive part represents the cohesion of the condensed phase. These interaction potentials are unsatisfactory for elemental semiconductors such as Si or Ge because the diamond structure is unstable when described by any reasonably smooth two-body potential. It is therefore essential to include three-body interactions to take into account the covalent interactions in elemental semiconductors.[45,61]

The situation is different in AX_2 (A=Si or Ge and X=O, S, Se, and Te) -type semiconductors and insulators. There is a charge transfer from A to X, resulting in the formation of A^{4+} and X^{2-} ions in the condensed phase. As a result of charge transfer, A^{4+} ions are considerably smaller than X^{2-} ions. Thus, the two-body interaction potentials for these systems should include at least steric repulsion and long-range Coulomb interactions. The most primitive model to include these essential interactions is the charged hard-sphere model, provided the ratio of the atomic sizes is greater than a critical value ($\sigma_x/\sigma_A \geq 2.44$).[62] Since the negative ions such as O^{2-}, S^{2-}, Se^{2-}, and Te^{2-} are among the largest in the Periodic Table and thus highly polarizable, the electronic polarizability of these ions is an important term in the interaction potential. In addition, covalent interactions, which are essential in materials such as Si, Ge, S, and Se, are also important for AX_2-type materials.

Recently, we have developed interaction potentials for MD simulations of AX_2-type glasses. These potentials include two- and three-body interactions:

$$V=\sum_{1\leq i<j\leq N} V_2(r_{ij})+\sum_{1\leq i\leq j\leq k\leq N} V_3(\mathbf{r}_{ij},\mathbf{r}_{jk},\mathbf{r}_{ik}) . \quad (1)$$

The two-body part of the potential, V_2, consists of three terms: (1) Steric repulsion due to ionic sizes, (2) Coulomb interactions to take into account charge transfer, and (3) charge-dipole interaction to include the effect of electronic polarizabilities. We use the form

$$V_2=\frac{H_{ij}}{r^{\eta_{ij}}}+\frac{Z_iZ_j}{r}-\frac{\frac{1}{2}(\alpha_iZ_j^2+\alpha_jZ_i^2)}{r^4}e^{-r/r_{4s}} , \quad (2)$$

where H_{ij} and η_{ij} are the strengths and exponents of the steric repulsion, and Z_i and α_i represent the effective charge and electronic polarizability of the ith ion, respectively. For A^{4+} and X^{2-} the effective charges are $+4Q$ and $-2Q$, respectively, where Q is the unit of charge transfer. The exponential screening term in the charge-dipole interaction provides a reasonable cutoff for the r^{-4} interaction. The value of the decay length r_{4s} is taken to be a few Å so that the magnitude of the charge-dipole potential at the edge ($L/2$) of the MD cell is reduced to a few percent of the charge-dipole potential without the exponential term.

Although there are six three-body terms in the interaction potential or AX_2-type systems, the two most important terms involve X—A—X and A—X—A because A—X is the smallest bond with the strongest attractive energy. The three-body X—A—X and A—X—A interactions include variations of A—X bond length, and of $\sphericalangle X$—A—X and $\sphericalangle A$—X—A bond angles. The expression for the three-body interaction is

$$V_3=B_{jik}f(r_{ij},r_{ik})p(\theta_{jik},\bar{\theta}_{jik}) , \quad (3)$$

where B_{jik} is the strength of the three-body interaction, the functions $f(r_{ij},r_{ik})$ represent the effects of bond stretching, and $p(\theta_{jik},\bar{\theta}_{jik})$ the effects of bond bending.

TABLE II. Constants in the interaction potential for SiO_2, Eqs. (1)–(5). Unit of length is Å and of energy $e^2/Å=14.39$ eV. Z is the effective charge, α the electronic polarizability (which has the dimension of volume), η the repulsive exponents, and H the repulsive strength. The constants B, l, $\bar{\theta}$, and r_0 pertain to the three-body part of the interaction potential, where B is the strength, and l, $\bar{\theta}$, and r_0 are constants defined in Eqs. (4) and (5). The range of the three-body interactions is $\leq r_0$.

	Z	α
Si	1.60	0.00
O	−0.80	2.40
	η	H
Si-Si	11	0.057
Si-O	9	11.387
O-O	7	51.692

	B	l	$\bar{\theta}$	r_0
A-X-A	1.40	1.0	141.00	2.60
X-A-X	0.35	1.0	109.47	2.60

We define $r_{ij}=|\mathbf{r}_i-\mathbf{r}_j|$ and θ_{jik} as the angle subtended by $\mathbf{r}_{ji}$ and $\mathbf{r}_{ki}$ at the vertex at i. The three-body contribution vanishes when the angle θ_{jik} is equal to $\bar{\theta}_{jik}$, and is positive otherwise. Thus the angle-dependent part, $p(\theta_{jik},\bar{\theta}_{jik})$ of Eq. (3) discriminates in favor of pair of bonds with desired geometry emanating from the vertex i. The expressions for $f(r_{ij},r_{ik})$ and $p(\theta_{jik},\bar{\theta}_{jik})$ read

$$f(r_{ij},r_{ik})=\begin{cases}\exp\left[\dfrac{l}{r_{ij}-r_0}+\dfrac{l}{r_{ik}-r_0}\right] & \text{for } r_{ij},r_{ik}<r_0\\ 0 \quad \text{for } r_{ij},r_{ik}>r_0\ , & \end{cases} \tag{4}$$

$$p(\theta_{jik},\bar{\theta}_{jik})=(\cos\theta_{jik}-\cos\bar{\theta}_{jik})^2\ , \tag{5}$$

where r_0 is the cutoff distance for the three-body interaction. The form in Eq. (4) automatically cuts off the interaction when r_{ij} or $r_{ik}=r_0$, with no discontinuities in the derivatives with respect to r.

In the three-body X-A-X and A-X-A interactions, the radial part, $f(r_{ij},r_{ik})$, is the same, but the angular part $p(\theta_{jik},\bar{\theta}_{jik})$ is different due to different values of the angles $\bar{\theta}_{XAX}$ and $\bar{\theta}_{AXA}$. The strengths of the three-body interactions (B_{XAX} and B_{AXA}) are, of course, different.

The constants in the interaction potentials were determined in two steps. First, from our earlier experience with superionic conductors[63] and glasses,[64,65] the exponents η_{AA},η_{AX}, and η_{XX} in the two-body part were taken to be 11, 9, and 7, respectively. Since the size of X^{2-} ions is much larger than that of A^{4+} ions and the dimension of the electronic polarizability is volume, we neglect the electronic polarizability of A^{4+} ions, $\alpha_{A^{4+}}=0$, and used the experimental value of $\alpha_{X^{2-}}$ taken from standard tables;[66] r_{4s} is chosen to be 4.43 Å. The remaining constants, i.e., the strengths of steric repulsions and effective charge are determined from the melting temperature and pressure at the experimental density. Among the repulsive constants, H_{AA} is the least important because A^{4+} ions are small and A^{4+}-A^{4+} interaction has the strongest Coulomb repulsion. The optimum values of B_{XAX} and B_{AXA} in the three-body interactions are listed in Table II. No adjustment of the two-body part was made when three-body interactions were incorporated. The values of all the constants in the interaction potential are given in Table II. The two-body contributions to the interaction potentials, Eq. (2), for SiO_2 are shown in Fig. 1.

III. ENERGIES OF CRYSTALLINE STRUCTURES

Energies of some of the commonly occurring crystalline forms of SiO_2 were calculated with the proposed interaction potential, Eqs. (1)–(5). The crystalline structures we investigated include α- and β-cristobalites, α- and β-quartz, keatite, and ideal β-cristobalite. The essential information about these structures is given in Table I. Ideal β-cristobalite can be obtained by starting from the diamond structure of Si and introducing oxygen atoms at the midpoint of neighboring Si atoms. However, this structure is dynamically unstable and not found in nature because the Si—O—Si lie on a straight line. The energy for ideal β-cristobalite is included for the purpose of illustration only.

The density dependence of the energy of the above-mentioned structures is shown in Fig. 2. The lowest-energy structures are α-cristobalite and α-quartz. These structures are nearly degenerate in energy, although their densities differ by 12%. The densities at the minima for α-cristobalite and α-quartz are 7.16×10^{22} and 8.03×10^{22} cm^{-3}, respectively, and the corresponding experimental values are 7.088×10^{22} cm^{-3} (=2.35 g/cm^3) and 7.956×10^{22} cm^{-3} (=2.65 g/cm^3). Experimentally, α-cristobalite and α-quartz are also the lowest-energy structures found in nature. At high temperatures and normal pressure, α-cristobalite and α-quartz transform into corresponding β-structures at $T=490$–530 (Ref. 4) and 840 K,[3] respectively. The energies of β-cristobalite and β-quartz are higher than those of α-cristobalite and α-quartz. The energy of ideal β-cristobalite is higher

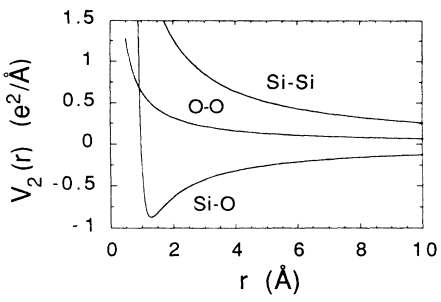

FIG. 1. Si-Si, Si-O, and O-O contributions to the two-body part of the interaction potentials, Eq. (2), for SiO_2. Total interaction potential is a sum of two-body, Eq. (2), and three-body contributions, Eq. (3). Unit of length is Å and of energy $e^2/\text{Å}=14.39$ eV.

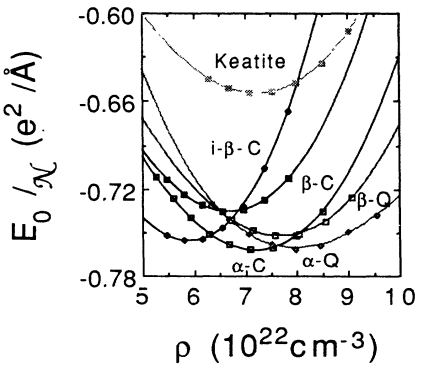

FIG. 2. Total potential energy (two plus three body) per particle, $E_0/\mathcal{N}$ in units of $e^2/\text{Å}=14.39$ eV, for various crystalline phases of SiO_2 as a function of density: ideal β-cristobalite (i-β-C), β-cristobalite (β-C), α-cristobalite (α-C), β-quartz (β-Q), α-quartz (α-Q), and keatite.

than those of α-cristobalite and α-quartz. Although the energy of ideal β-cristobalite is lower than that of real β-cristobalite, the density of the ideal structure is much lower than the experimental value and it is dynamically unstable. The energy of keatite is higher than those of cristobalite and quartz structures. The energy minimum for keatite occurs at 7.22×10^{22} cm^{-3}, in good agreement with the experimental value 7.526×10^{22} cm^{-3} (see Table I).

IV. MOLECULAR-DYNAMICS CALCULATION AND THE PREPARATION OF VITREOUS STATES

A. Molecular-dynamics method

Molecular-dynamics calculations were performed for systems of 648 and 5184 particles with periodic-boundary conditions. The number density in the simulation (6.62×10^{22} cm^{-3}) corresponds to the experimental value 2.20 g/cm^3 for a-SiO_2. The length of the MD box was 21.392 Å for 648-particle system and 42.782 Å for 5184-particle systems, respectively. Long-range Coulomb interactions were treated with Ewald's summation. The equations of motion were integrated with an algorithm due to Beeman and Alben[67] using a time step of 0.5×10^{-15} sec. The total energy of the system was conserved to better than 1 part in 10^4 over the entire simulation.

B. Characterization of molten states

Starting from a random configuration, the system was heated to a temperature of 3000 K and equilibrated for a long time (60 000 time steps) so that the initial state has no effect on the system at 3000 K. The system at 3000 K was run for an additional 30 000 time steps and the averages were evaluated over two segments of 15 000 time steps each. Within statistical uncertainty, the averages over these two segments are found to be the same. The long simulations are necessary because the relaxation is much slower with the inclusion of three-body forces. The system at 3000 K was cooled to 2500 K, equilibrated for 30 000 time steps, and again the averages were calculated over an additional 15 000 time steps. Using the same cooling schedule, a system at 2000 K was obtained. In addition a system at 3500 K was prepared by heating the 3000-K system.

The constants of self-diffusion were calculated from mean-square dispacements,

$$\langle r^2\rangle_\alpha=\left\langle\frac{1}{\mathcal{N}_\alpha}\sum_{j(\alpha)}[\mathbf{r}_j(t+s)-\mathbf{r}_j(s)]^2\right\rangle , \tag{6}$$

$$D_\alpha=\lim_{t\to\infty}(\langle r^2\rangle_\alpha/6t) , \tag{7}$$

and velocity autocorrelation functions,

$$D_\alpha=\frac{k_BT}{m_\alpha}\int_0^\infty Z_\alpha(t)dt , \tag{8}$$

$$Z_\alpha(t)=\frac{\langle\mathbf{v}_i(0)\cdot\mathbf{v}_i(t)\rangle_\alpha}{\langle v_i^2(0)\rangle_\alpha} , \tag{9}$$

where $\mathcal{N}_\alpha$ and m_α are the number of particles and mass of the αth species. The values of the constant of self-diffusion obtained by these two methods are in satisfactory agreement with each other. The total energy per particle and the constants of self-diffusion for Si and O at these four temperatures are shown in Figs. 3(a) and 3(b), respectively. Finite diffusivities for Si and O indicate that the systems at these temperatures are in the molten state. However, the small values of diffusion constants at 2000 K suggest that this system is close to freezing.

The molten state 2000 K was quenched and thermalized at a rate of 0.1% per 10 Δt, leading to a state at 1500 K. At this temperature, long-range diffusion ceases and the system undergoes thermal arrest. However, local rearrangements continue to take place because of considerable thermal energy in the system. This system was thermalized for 30 000 time steps and then the averages were accumulated over an additional 30 000 time steps. A schematic of the cooling and thermalization schedule is given in Fig. 4. Using similar cooling and thermalization schedules, systems at 600, 300, and 0 K were obtained. The total energy per particle for these three states are also shown in Fig. 3(a). The constants of self-diffusion at 600, 300, and 0 K are negligible ($<10^{-7}$ cm^2/sec).

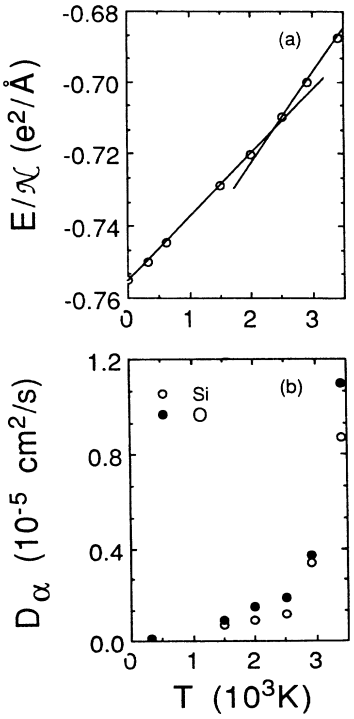

FIG. 3. (a) Total internal energy per particle, $E/\mathcal{N}$, in units of $e^2/\text{Å}=14.39$ eV, vs temperature T, for amorphous and molten SiO_2. The results for amorphous and molten states are for fixed number density 6.62×10^{22} cm^{-3} ($=2.20$ g/cm^3). The change in slope at high temperature to low temperature indicates the onset of structural arrest. (b) Constants of self-diffusion for silicon and oxygen vs temperature.

C. Structural correlation functions

Molecular-dynamics trajectories provide complete information on structural and dynamical correlations. In this paper, we have examined two-body structural correlations through pair-distribution functions and static structure factors, and three-body correlations through bond-angle distributions.

Partial pair-distribution functions are calculated from

$$\langle n_{\alpha\beta}(r)\rangle \Delta r = 4\pi r^2 \Delta r \, \rho c_\beta g_{\alpha\beta}(r) , \tag{10}$$

where $n_{\alpha\beta}(r)\Delta r$ denotes the number of particles of species β in a shell between r and $r+\Delta r$ around a particle of species α. The angular brackets represent the ensemble average and an average over all the particles of species α. ρ is the total number density ($=\mathcal{N}/\Omega$, $\mathcal{N}=\mathcal{N}_\alpha+\mathcal{N}_\beta$) and $c_\beta=\mathcal{N}_\beta/\mathcal{N}$ is the concentration of species β.

The coordination number $N_{\alpha\beta}(R)$ is an integral over the corresponding partial pair-distribution function:

$$N_{\alpha\beta}(R)=4\pi\rho c_\beta \int_0^R g_{\alpha\beta}(r) r^2 \, dr . \tag{11}$$

$N_{\alpha\beta}(R)$ gives the number of particles of species β around an α in a sphere of radius R. The total pair-distribution function $g(r)$ is defined as

$$g(r)=\sum_{\alpha,\beta} c_\alpha c_\beta g_{\alpha\beta}(r) . \tag{12}$$

Partial static structure factors are calculated from the Fourier transforms of corresponding partial pair-distribution functions:

$$S_{\alpha\beta}(q)=\delta_{\alpha\beta}+4\pi\rho(c_\alpha c_\beta)^{1/2} \times \int_0^\infty [g_{\alpha\beta}(r)-1]\frac{\sin(qr)}{qr} r^2 \, dr , \tag{13}$$

and the total static structure factor is given by

$$S(q)=\sum_{\alpha,\beta}(c_\alpha c_\beta)^{1/2} S_{\alpha\beta}(q) . \tag{14}$$

In a neutral system, the structural information about two-body correlations is completely determined by the above-mentioned correlation functions. However, in systems with charge-transfer effects, it is also instructive to examine two-body charge-charge correlations. In this paper, we investigate both the density-density static structure factor, $S(q)$ and charge-charge static structure factor $S_{ZZ}(q)$, defined as

$$S_{ZZ}(q)=\frac{\sum_{\alpha,\beta} Z_\alpha Z_\beta (c_\alpha c_\beta)^{1/2} S_{\alpha\beta}(q)}{\sum_\alpha Z_\alpha^2 c_\alpha} . \tag{15}$$

The corresponding charge-charge pair-distribution function is then

$$g_{ZZ}(r)=\frac{\sum_{\alpha,\beta} Z_\alpha Z_\beta c_\alpha c_\beta g_{\alpha\beta}(r)}{\sum_\alpha Z_\alpha^2 c_\alpha} . \tag{16}$$

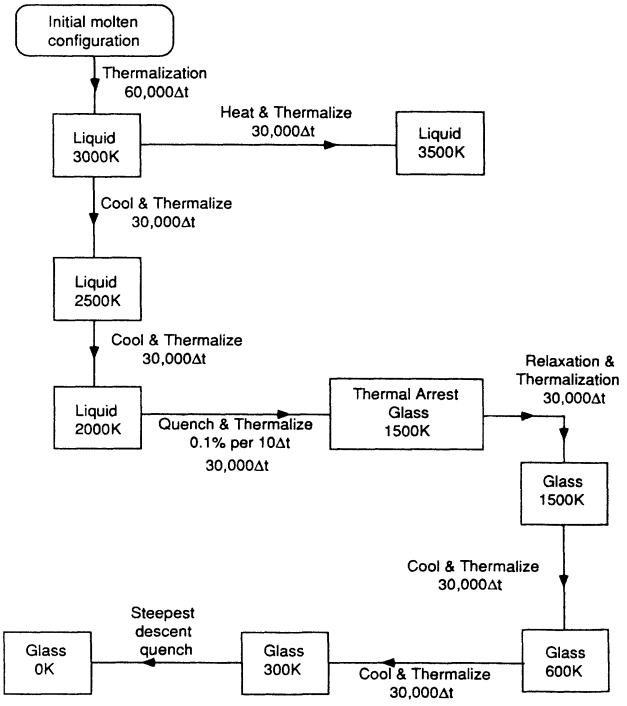

FIG. 4. Schematic diagram of quenching and thermalization schedules used in MD simulations for preparing SiO_2 glass from a well-thermalized molten state. Measurements were made for 30 000 steps (15 000+15 000) in each state indicated in the boxes. Steepest-descent quench is a mathematically well-defined procedure to find the nearest local minimum of the system (Refs. 68 and 69).

D. Neutron-scattering correlation functions

The neutron-scattering static structure factor can be obtained from the partial static structure factors by weighting them with coherent neutron-scattering lengths:[70]

$$S_N(q)=\frac{\sum_{\alpha,\beta} b_\alpha b_\beta (c_\alpha c_\beta)^{1/2}[S_{\alpha\beta}(q)-\delta_{\alpha\beta}+(c_\alpha c_\beta)^{1/2}]}{\left[\sum_\alpha b_\alpha c_\alpha\right]^2} , \tag{17}$$

where b_α denotes the coherent neutron-scattering length of species α. The other structural correlation functions that are often used in the analysis of neutron-diffraction data are $g_N(r)$, $t(r)$, $d(r)$, and $qI_N(q)$. We define these quantities as follows:

$$g_N(r)=\frac{\sum_{\alpha,\beta} c_\alpha b_\alpha c_\beta b_\beta g_{\alpha\beta}(r)}{\left[\sum_\alpha b_\alpha c_\alpha\right]^2} , \tag{18}$$

$$t(r)=4\pi\rho r g_N(r) , \tag{19}$$

$$d(r)=t(r)-4\pi\rho r , \tag{20}$$

$$qI_N(q)=\int_0^\infty d(r)\sin(qr)dr$$
$$=q[S_N(q)-1] . \tag{21}$$

Slightly different definitions of neutron-scattering correlations are used by different groups.[26,71]

E. Bond angle distributions

Bond-angle distributions are obtained from MD trajectories as follows: Let us first consider the case of an X—A—X bond angle distribution. In this case, a list of nearest-neighbor atoms of type X around an A atom is constructed. This requires a cutoff distance for A-X separation which is taken to be the position of the first minimum in $g_{AX}(r)$. From this nearest-neighbor list for each A atom, the angles $\sphericalangle X$—A—X are calculated for all bonds and a histogram is then constructed from an average over all angles involving all A atoms. Next, let us consider an A—A—X bond-angle distribution. In this case, two nearest-neighbor distance lists involving atoms A and X around each A atom are constructed. The cutoff distances are the first minima in $g_{AA}(r)$ and $g_{AX}(r)$. Then a histogram is constructed from all A—A—X angles.

V. RESULTS

Atomic trajectories from MD simulations are used to calculate a variety of positional and angular correlations in molten and vitreous SiO_2. The calculation for vitreous and molten states are carried out at a fixed number density of 6.62×10^{22} cm^{-3} ($=2.20$ g/cm^3). Short- and intermediate-range order in the system are then inferred from these correlation functions. A detailed comparison of the MD results is made with diffraction and NMR measurements. The origin of the first sharp diffraction peak (FSDP) is traced through partial static structure factors and from a comparison between density-density and charge-charge correlation functions.

A. Short-range order

The partial pair-distribution functions and bond-angle distributions are used to determine the short-range order. Figures 5 and 6 show the MD results for Si-Si, Si-O, and O-O pair-distribution functions in the glass and molten states, respectively. In the glass, the position of the first peak in $g_{SiO}(r)$ gives the Si—O bond length to be 1.62 ± 0.02 Å. The corresponding experimental value from recent neutron-diffraction data is 1.61 ± 0.05 Å. From the area under the first peak, the nearest-neighbor coordination of Si is found to be 4 and of O to be 2, in accordance with the $8-n$ rule. The position of the first peak in $g_{SiO}(r)$ remains at 1.62 Å in the molten state, although the pair-distribution function is broader than that of the amorphous state.

The nearest-neighbor O-O distance from Fig. 5 is

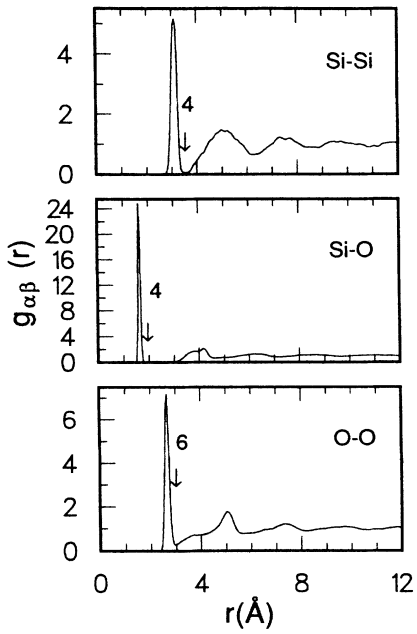

FIG. 5. Partial pair-distribution functions $g_{\alpha\beta}(r)$ vs r in SiO_2 glass at 310 K. The arrows indicate the coordination numbers.

2.64 ± 0.02 Å and the corresponding experimental value,[13] inferred from neutron-diffraction data, is 2.632 ± 0.089 Å. The average value of O-O separation remains at 2.64 Å in the molten state, although the width of the first peak in $g_{OO}(r)$ shows the expected thermal

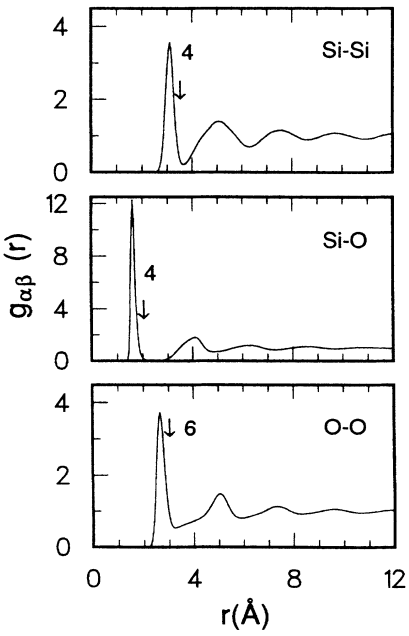

FIG. 6. Partial pair-distribution functions $g_{\alpha\beta}(r)$ vs r in molten SiO_2 at 2500 K. The arrows indicate the coordination numbers.

TABLE III. Molecular-dynamics results for the bond lengths and full width at half maximum (FWHM) for a-SiO_2 and molten SiO_2.

	Glass (310 K)		Liquid (2500 K)	
	Bond length (Å)	FWHM (Å)	Bond length (Å)	FWHM (Å)
Si—O	1.62	0.05	1.62	0.15
O—O	2.64	0.15	2.64	0.35
Si—Si	3.10	0.20	3.15	0.30

broadening. From the area under the first peak in $g_{OO}(r)$ we determine that each O on the average has six nearest-neighbor O atoms, in accordance with neutron experiments.[13] Molecular-dynamics results for the bond lengths and full widths at half maximum (FWHM) for a-SiO_2 and molten SiO_2 are summarized in Table III.

The bond-angle distributions in the amorphous and molten SiO_2 are shown in Figs. 7 and 8, respectively. The angle distribution for $\sphericalangle$O—Si—O is peaked at 109° with a full width at half maximum (FWHM) of 10° in the glass at 310 K and 14° in the molten state at 2500 K. The first peak in the $\sphericalangle$O—O—O distribution occurs at 60° in the amorphous as well as the molten states. The facts that each Si has four nearest-neighbor O atoms and that $\sphericalangle$O—Si—O and $\sphericalangle$O—O—O distributions have peaks at 109° and 60°, respectively, establish the presence of $Si(O_{1/2})_4$ tetrahedra. These tetrahedra are nearly perfect and are present in the molten state as well. It should also be noted that for perfect $Si(O_{1/2})_4$ tetrahedra O—O—Si angle is 35.26° and, indeed, the corresponding bond-angle distributions in Figs. 7 and 8 are peaked around 35°.

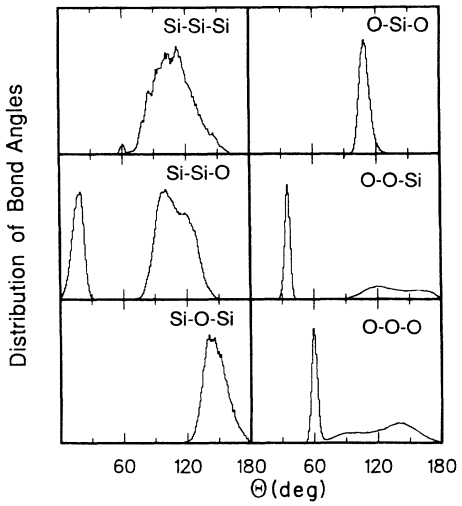

FIG. 7. Distribution of bond angles for a-SiO_2 at 310 K. The O—Si—O distribution has a peak at 109° with a FWHM of 10°. The Si—O—Si distribution is peaked around 142° with a FWHM of 25°.

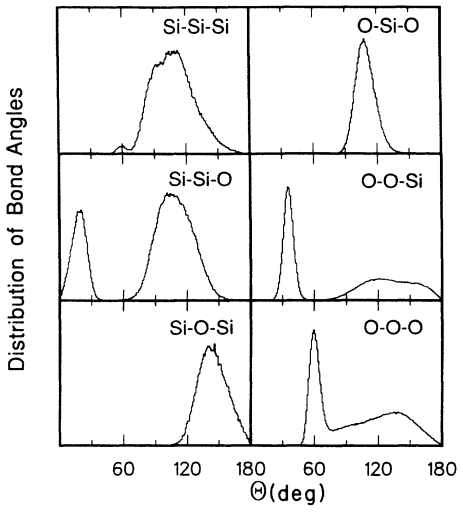

FIG. 8. Distribution of bond angles in molten SiO_2 at 2500 K. The O—Si—O distribution has a peak at 109° with a FWHM of 14°. The Si—O—Si distribution is peaked around 142° with a FWHM of 34°.

B. Connectivity of $Si(O_{1/2})_4$ tetrahedra

The $\sphericalangle$Si—O—Si bond-angle distributions in Figs. 7 and 8 reveal how the nearest-neighbor tetrahedra are connected to one another. For angles less than 120 ° the distribution is zero, indicating that there are no edge-sharing tetrahedra (two-fold rings) in the system. All the tetrahedra are joined at corners. The $\sphericalangle$Si—O—Si distribution peaks around 142° with a FWHM of 25° in the glass at 310 K. Mozzi and Warren[9] have determined the $\sphericalangle$Si—O—Si bond-angle distribution using the x-ray-diffraction technique. They find a peak in the distribution of 144° with a FWHM of 38°. The distribution has no weight below 120°, thus ruling out the possibility of edge-sharing tetrahedra. Recent NMR measurement by Pettifer *et al.*[28] reveals that the peak in $\sphericalangle$Si—O—Si distribution is at 142° and the FWHM is 26°. From the MD results we determine that the $\sphericalangle$Si—O—Si distribution in the molten state at 2500 K is peaked around 142.5° with a FWHM of 34°. Table IV gives MD result for the bond angles and FWHM for a-SiO_2 and molten SiO_2.

It is interesting to note that theoretical calculations[72] on the ground-state structure of an isolated Si—O—Si molecule give the $\sphericalangle$Si—O—Si bond angle to be 136.4°.

TABLE IV. Molecular-dynamics results for the bond angles and full width at half maximum (FWHM) for a-SiO_2 and molten SiO_2.

	Glass (310 K)		Liquid (2500 K)	
	Bond angle (deg)	FWHM (deg)	Bond angle (deg)	FWHM (deg)
O—Si—O	109.6	10	109.5	14
Si—O—Si	142.0	25	142.5	34

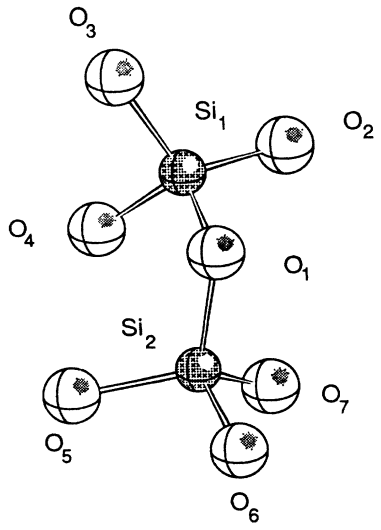

FIG. 9. A schematic view of corner-sharing tetrahedra in a-SiO_2.

This angle is not too different from the angles found in crystalline and amorphous states of SiO_2.

A typical pair of corner-sharing tetrahedra from our MD calculations for glass is shown in Fig. 9. With the calculated Si—O bond length of 1.62 Å and an Si—O—Si bond angle of 142°, one can explain the occurrence of various peaks in the partial pair-distribution functions. For instance, the Si-Si nearest-neighbor separation (Si_1-Si_2) is 3.06 Å, which explains the position of the first peak at 3.10 Å in $g_{Si\text{-}Si}(r)$. X-ray measurements, as quoted by Johnson *et al.*,[13] give the nearest-neighbor Si-Si separation in a-SiO_2 to be 3.08±0.10 Å. The Si-Si separation remains at 3.1 Å in the molten state.

The second-nearest-neighbor O-O separation [O(2)-O(7)] calculated from Fig. 9 is 4.86 Å. In $g_{OO}(r)$ shown in Fig. 5, the second peak indeed occurs at 5 Å. The corresponding O—O—O bond angle in Fig. 9 is found to be 134° and, in fact, a peak is observed at 134° in the O—O—O bond-angle distribution shown in Fig. 7. Finally, the Si—Si—Si bond-angle distributions in both Figs. 7 and 8 have peaks at 105 ° which, combined with the nearest-neighbor Si-Si separation of 3.10 Å, gives 4.92 Å for the second-nearest-neighbor Si-Si separation. The broad second peak in $g_{SiSi}(r)$ is observed at 5Å. The above analyses establish that all the important features in the partial pair-distribution functions can be understood on the basis of corner-sharing tetrahedra in the amorphous state.

C. Comparison with diffraction experiments

Structural correlations in a-SiO_2 have been investigated with both neutron- and x-ray-diffraction techniques. For a-SiO_2, the MD results (solid line) for the neutron static structure factor $S_N(q)$ and the recent experimental results of Johnson *et al.*[13] (solid circles) are shown in Fig. 10. The heights and widths of all the peaks in the MD results

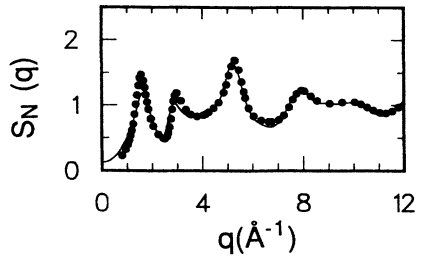

FIG. 10. Neutron static structure factor $S_N(q)$ for a-SiO_2. Solid line, MD results at 310 K; solid dots, neutron-diffraction experiments (Ref. 13) at 10 K.

for $S_N(q)$ are in excellent agreement with the neutron-diffraction measurements.

The origin of various peaks in $S_N(q)$ can be inferred from partial static structure factors calculated from MD trajectories. The results for partial static structure factors in a-SiO_2 are shown in Fig. 11. It is evident that the second peak in $S_N(q)$ involves contributions from Si-Si and O-O correlations with partial cancellation arising from Si-O anticorrelations. The third and fourth peaks receive contributions from Si-Si, Si-O, and O-O correlations. A small shoulder observed at 10 Å^{-1} in $S_N(q)$ consists of contributions mostly from O-O correlations.

The MD results for total pair-distribution functions with and without coherent neutron-scattering lengths are shown in Fig. 12. These distribution functions show peaks at 1.62, 2.64, 3.10, 3.85, 4.15, and 5.05 Å. The first three peaks reflect the nearest-neighbor Si-O, O-O, and

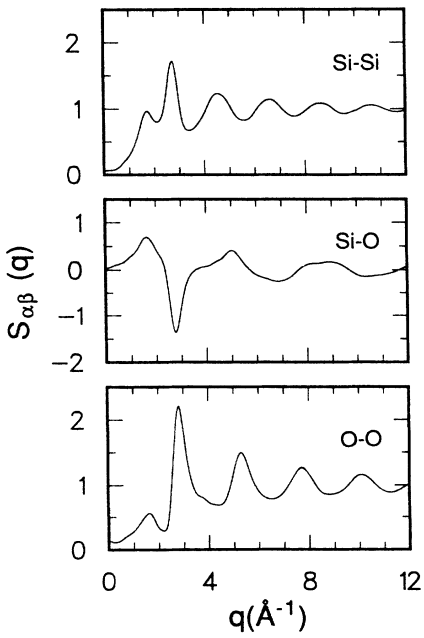

FIG. 11. Partial static structure factors $S_{\alpha\beta}(q)$ for a-SiO_2 at 310 K.

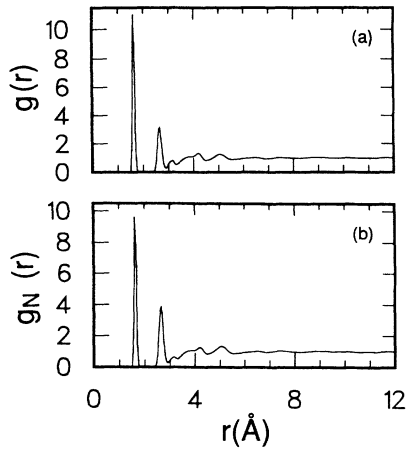

FIG. 12. (a) Total pair-distribution function $g(r)$, Eq. (12), and (b) total neutron pair-distribution function $g_N(r)$, Eq. (18), for a-SiO_2 at 310 K.

Si-Si separations, respectively. These nearest-neighbor distances are also manifested in correlation functions $t(r)$ and $d(r)$, shown in Fig. 13.

So far we have only discussed the positional correlations such as pair-distribution functions and static structure factors that arise from number-density fluctuations. In a system like SiO_2, where the charge-transfer effect is important, it is also instructive to investigate the nature of charge-density fluctuations. Using the MD results for partial static structure factors and the effective charges $+4Q$ and $-2Q$ for Si and O, respectively, we have calculated the charge-charge static structure factor, $S_{ZZ}(q)$, from Eq. (15). The results for $S_{ZZ}(q)$ and the corresponding charge-charge pair-distribution function, $g_{ZZ}(r)$, Eq. (16), in the glassy state at 310 K are shown in Figs. 14 and 15, respectively. The peaks in $S_{ZZ}(q)$ occur at 2.76, 4.35, 6.75, and 10.36 $Å^{-1}$. In the static structure factors $S(q)$, Eq. (14) and $S_N(q)$, Eq. (17), both of which

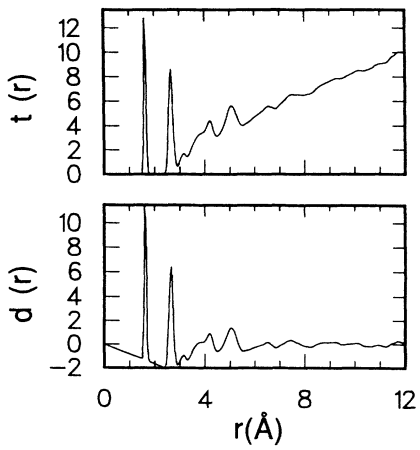

FIG. 13. MD results for $d(r)$, Eq. (19), and $t(r)$, Eq. (20), at 310 K.

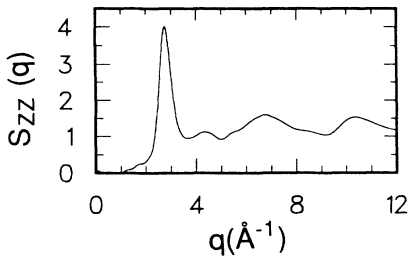

FIG. 14. Total charge-charge static structure factor $S_{ZZ}(q)$, Eq. (15), for a-SiO_2 at 310 K. The most important feature of this correlation function is the absence of the first sharp diffraction peak.

reflect number-density fluctuations, we find the first sharp diffraction peak at 1.55, and the subsequent peaks at 2.88, 5.16, and 7.90 $Å^{-1}$. The striking difference between $S(q)$ and $S_{ZZ}(q)$ is the absence of the FSDP in the latter. To understand the absence of the FSDP in $S_{ZZ}(q)$, it should be noted that the FSDP arises due to contributions from Si-Si, Si-O, and O-O as is evident from Fig. 11. In $S_{ZZ}(q)$ the factor multiplying the Si-O partial static structure factor is negative, whereas the factors multiplying Si-Si and O-O structure factors are positive. As a result, there is a large cancellation between Si-O, Si-Si, and O-O contributions, causing the near disappearance of the FSDP in the charge-charge static structure factor.

Partial static structure factors in Fig. 11 show that the second peaks in Si-Si and O-O occur at the same q as the largest minimum in Si-O. When weighted by the effective charges on Si and O, these maxima and the minimum in $S_{SiO}(q)$ add up and give rise to the second peak in $S_{ZZ}(q)$. The position of this peak in $S_{ZZ}(q)$ is essentially at the same position as the second peak in $S(q)$ or $S_N(q)$. In a similar fashion, it is easy to understand why the remaining features in $S_{ZZ}(q)$ are out of phase with those found in $S(q)$ or $S_n(q)$.

D. Intermediate-range order and the first sharp diffraction peak

The first sharp diffraction (FSDP) is a feature common to a variety of binary covalent glasses. These include SiO_2, GeO_2, As_2Se_3, $SiSe_2$, As_2S_3, etc. Diffraction measurements on these systems reveal that the position of the

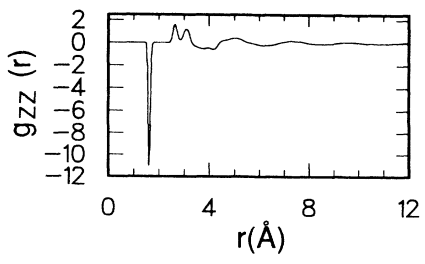

FIG. 15. Total charge-charge pair-distribution function $g_{ZZ}(r)$, Eq. (16), for a-SiO_2 at 310 K.

FSDP lies between 1.0 and 1.5Å^{-1}. In fact, the highest value corresponds to the FSDP position in a-SiO_2: Neutron- and x-ray-diffraction experiments observe the FSDP around 1.5 Å^{-1} and our simulations reveal the position of the FSDP to be around 1.55 Å^{-1}. Partial static structure factors, shown in Fig. 11, indicate that the FSDP consists of contributions from Si-Si, Si-O, and O-O correlations.

As regards the spatial extent of these correlations, it is clear from the total pair-distribution function $g(r)$ in Fig. 12 that the FSDP's cannot arise from correlations beyond 8 Å since $g(r)$ is almost unity beyond this distance. Below 4 Å the structure in $g(r)$ arises mainly from nearest-neighbor distances between Si-O (1.62 Å), O-O (2.64 Å), and Si-Si (3.10 Å). This leaves the correlations in the range 4–8 Å. We have calculated the structure factor from $g(r)$ by truncating correlations beyond a certain distance r_c:

$$S(q)=1+4\pi\rho\int_0^{r_c}[g(r)-1]\frac{r^2\sin(qr)}{qr}dr\ . \qquad (22)$$

We find that $r_c \geq 8$ Å has a negligible effect on the FSDP, but for $4<r_c<8$ Å the FSDP becomes rounded and its height is affected significantly. The sensitivity of the FSDP to these spatial correlations establishes the range of intermediate-range order to be between 4 and 8 Å.

This information regarding the FSDP derived from the static structure factor and corresponding pair-distribution function, when combined with the fact that the FSDP is absent in $S_{ZZ}(q)$, leads to a much deeper understanding of the origin of FSDP's in covalent glasses. First of all, it should be stressed that in a-$GeSe_2$ and a-$SiSe_2$, which have different connectivities than a-SiO_2, the FSDP also arises from density-density correlations in the range 4–8 Å.[65] Furthermore, the FSDP is also absent in the $S_{ZZ}(q)$ for a-$GeSe_2$ and a-$SiSe_2$. Also, when only two-body interactions are used to describe the glassy state in a-$GeSe_2$ with the hypernetted-chain-approximation (HNC) scheme, the FSDP is absent in $S_{ZZ}(q)$, but not in $S(q)$.[64] The point to be emphasized here is that *the absence of the FSDP in $S_{ZZ}(q)$ is independent of the interaction potential used to describe the system, or the particular detail of the connectivity of the system, or the theoretical scheme used to carry out the calculations.*

The analyses of the origin of the FSDP form $S(q)$ and

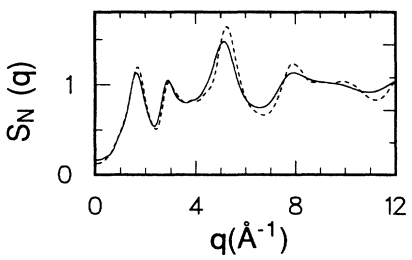

FIG. 16. MD results for the neutron static structure $S_N(q)$ for molten SiO_2 at 2500 K. Solid line is for the molten state and dashed for glass at 310 K.

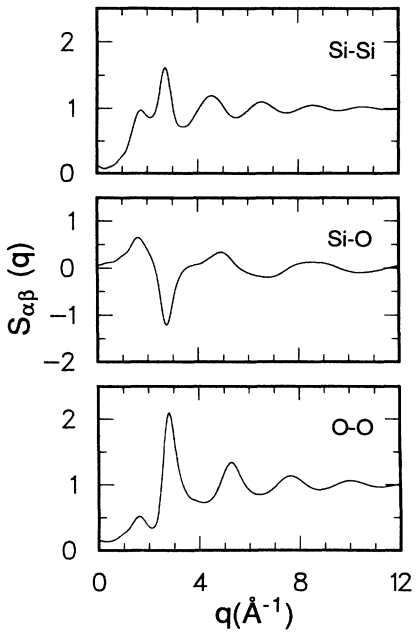

FIG. 17. MD results for partial neutron static structure factor $S_{\alpha\beta}(q)$ for molten SiO_2 at 2500.

$S_{ZZ}(q)$ imply that the FSDP results from correlations in the range 4–8 Å. These correlations are such that there are no charge-density fluctuations arising in the 4–8 Å range. In other words, charge neutrality prevails in the range 4–8 Å in these covalent glasses.

E. Static structure factor for the molten state

The neutron static structure factor $S_N(q)$ for molten SiO_2 at 2500 K is shown in Fig. 16. Corresponding partial static structure factors for the molten state are shown in Fig. 17.

To the best of our knowledge there is no neutron-diffraction experiment available for molten SiO_2. The general features of $S_N(q)$ in the molten state are as follows: The height of the FSDP is reduced and the width of the peak increases when compared to the result for the glassy state at 310 K. Other peaks in $S_N(q)$ and $S_{\alpha\beta}(q)$ in Fig. 17 also show reduced height and thermal broadening. The x-ray structure factor can easily be computed from $S_{\alpha\beta}(q)$ by multiplying them with appropriate form factors. The molten-state structure factor displays all the features found in the structure factor for a-SiO_2. Results for partial static structure factors in the molten state, shown in Fig. 17, indicate that the first sharp diffraction peak in $S_N(q)$ is due to Si-Si, Si-O, and O-O correlations, the second peak arises from Si-Si and O-O correlations with partial cancellation from Si-O anticorrelations, and the third peak is due to all three correlations, etc.

VI. CONCLUSION

In this paper, we have investigated the structural properties of a-SiO_2 using the molecular-dynamics technique.

The calculations are based on an effective potential consisting of two- and three-body terms. The two-body potential consists of Coulomb interaction, steric repulsion, and charge-dipole contributions. The three-body term comprises angle-dependent interactions involving Si—O—Si and O—Si—O angles, and variations in Si—O bond length. Our results for the static structure factor are in very good agreement with the neutron-diffraction experiments.[13] The MD results reveal that a-SiO_2 consists of $Si(O_{1/2})_4$ tetrahedra sharing corners, with the Si—O—Si bond-angle distribution peaking around 142° and having a FWHM of 25°. Recent NMR measurements[28] determine the peak in Si-O-Si distribution to be at 142° with a FWHM of 26°.

In molecular-dynamics results for the static structure factor, the first sharp diffraction peak occurs around 1.55 $Å^{-1}$, which is in good agreement with diffraction measurements. The simulations also show that the FSDP arises from Si-Si, Si-O, and O-O correlations in the range 4–8 Å and the absence of a FSDP in charge-charge structure factor implies that charge neutrality prevails over the length scale responsible for a FSDP.

We have also investigated structural correlations in molten SiO_2. The short-range order in the molten state is also dominated by $Si(O_{1/2})_4$ tetrahedra. These tetrahedra are corner sharing, and the Si—O—Si bond-angle distribution has a peak at 142.5°, while in a-SiO_2 this angle is 142°. Owing to increased thermal effects the FWHM is considerably broader, 34° compared to 25° in the vitreous state at 310 K. The persistence of intermediate-range order, signified by the FSDP, is somewhat surprising in sufficiently high-temperature molten states, and it should be investigated by diffraction experiments.

ACKNOWLEDGMENTS

We would like to thank our colleagues Dr. M. Grimsditch, Dr. D. L. Price, and Dr. S. Susman for many stimulating discussions, valuable advice, and for providing us with a wealth of unpublished experimental results. We also acknowledge many fruitful conversations with Dr. G. A. Antonio, Dr. H. Iyetomi, and Dr. M. Degani. We thank Dr. L. A. Curtis for providing us with his unpublished results on the ground-state configurations of Si—O—Si molecule. One of us (J. P. R.) would like to acknowledge the financial support from CnPq (Conselho Nacional de Desenvolvimento Científico e Tecnológico, Brazil), and the hospitality of the Materials Science Division at Argonne National Laboratory; and another (I.E.) would like to thank the Swedish Research Council and Argonne National Laboratory for their support. This work was supported by the U.S. Department of Energy (Division of Materials Science of the Office of Basic Energy Sciences) under Contract No. W-31-109-ENG-38. We would like to acknowledge a grant of computer time on Energy Research Cray supercomputers at the National Magnetic Fusion Energy Computing Center (Livermore, CA).

*Permanent address: Universidade Federal de São Carlos (UFSCar), via Washington Luiz Km. 235, Caixa Postal 676, 13 560 São Carlos, São Paulo, Brazil.

[1] *Physics of Disordered Materials,* edited by D. Adler, H. Fritzsche, and S. R. Ovshinsky (Plenum, New York, 1985); *The Physics and Technology of Amorphous SiO_2,* edited by R. A. B. Devine (Plenum, New York, 1988).

[2] F. Liebau, in *The Physics and Technology of Amorphous SiO_2,* edited by R. A. B. Devine (Plenum, New York, 1988), p. 15.

[3] R. W. G. Wyckoff, *Crystal Structures Vol. 1* (Wiley, New York, 1965).

[4] J. J. Pluth, J. V. Smith, and J. Faber, Jr., J. Appl. Phys. **57**, 1045 (1985).

[5] L. Levien, C. T. Prewitt, and D. J. Weidner, Am. Miner. **65**, 920 (1980).

[6] L. Levien and C. T. Prewitt, Am. Miner. **66**, 324 (1981).

[7] S. Tsunneyuki, M. Tsukada, H. Aoki, and Y. Matsui, Phys. Rev. Lett. **61**, 869 (1988); L. L. Liu, W. A. Bassett, and T. Takahashi, J. Geol. Res. **79**, 1160 (1974).

[8] J. A. E. Desa, A. C. Wright, J. Wong, and R. N. Sinclair, J. Non-Cryst. Solids **51**, 57 (1982).

[9] B. E. Warren, H. Krutter, and O. Morningstar, J. Am. Ceram. Soc. **19**, 202 (1936); R. L. Mozzi and B. E. Warren, J. Appl. Crystallogr. **2**, 164 (1969).

[10] A. C. Wright and A. J. Leadbetter, Phys. Chem. Glasses **17**, 122 (1976).

[11] R. N. Sinclair, J. A. E. Desa, G. Etherington, P. A. V. Johnson, and A. C. Wright, J. Non-Cryst. Solids **42**, 107 (1980).

[12] M. Misawa, D. L. Price, and K. Suzuki, J. Non-Cryst. Solids **37**, 85 (1980).

[13] P. A. V. Johnson, A. C. Wright, and R. N. Sinclair, J. Non-Cryst. Solids **58**, 109 (1983).

[14] R. N. Sinclair and A. C. Wright, J. Non-Cryst. Solids **57**, 447 (1983).

[15] F.L. Galeener, A. J. Leadbetter, and M. W. Stringfellow, Phys. Rev. B **27**, 1052 (1983).

[16] U. Buchenau, N. Nücker, and A. J. Dianoux, Phys. Rev. Lett. **53**, 2316 (1984).

[17] J. M. Carpenter and D. L. Price, Phys. Rev. Lett. **54**, 441 (1985).

[18] A. C. Wright and R. N. Sinclair, J. Non-Cryst. Solids **76**, 351 (1985).

[19] S. C. Moss and D. L. Price, in *Physics of Disordered Materials,* edited by D. Adler, H. Fritzsche, and S. R. Ovshinsky (Plenum, New York, 1985), p. 77.

[20] R. W. Johnson, D. L. Price, S. Susman, M. Arai, T. I. Morrison, and G. K. Shenoy, J. Non-Cryst. Solids **83**, 251 (1986).

[21] U. Buchenau, M. Prager, N. Nücker, and A. J. Dianoux, Phys. Rev. B **34**, 5665 (1986).

[22] D. L. Price and J. M. Carpenter, J. Non-Cryst. Solids **92**, 153 (1987).

[23] D. L. Price, S. Susman, and A. C. Wright, J. Non-Cryst. Solids **97&98**, 167 (1987).

[24] U. Walter, D. L. Price, S. Susman, and K. J. Volin, Phys. Rev. B **37**, 4232 (1988).

[25] M. Arai, D. L. Price, S. Susman, K. J. Volin, and U. Walter, Phys. Rev. B **37**, 4240 (1988).

[26] A. C. Wright, J. Non-Cryst. Solids **106**, 1 (1988).

[27] R. Dupree and R. F. Pettifer, Nature (London) **308**, 523

(1984).
[28]R. F. Pettifer, R. Dupree, I. Farnan, and U. Sternberg, J. Non-Cryst. Solids **106**, 408 (1988).
[29]A. E. Geissberg and F. L. Galeener, Phys. Rev. B **28**, 3266 (1983).
[30]F. L. Galeener and G. Lucovsky, Phys. Rev. Lett. **37**, 1474 (1976).
[31]F. L. Galeener, G. Lucovsky, and R. H. Geils, Solid State Commun. **25**, 405 (1978).
[32]R. J. Hemley, H. K. Mao, P. M. Bell, and B. O. Mysen, Phys. Rev. Lett. **57**, 747 (1986).
[33]P. H. Gaskell and D. W. Johnson, J. Non-Cryst. Solids **20**, 153 (1976); **20**, 171 (1976).
[34]J. D. Jorgensen, J. Appl. Phys. **49**, 5473 (1978).
[35]A. Polian and M. Grimsditch, Phys. Rev. B **27**, 6409 (1983); M. Grimsditch, *ibid.* **34**, 4372 (1986).
[36]M. Grimsditch, Phys. Rev. Lett. **52**, 2379 (1984).
[37]M. Ocaña, V. Fornés, and C. J. Serna, J. Non-Cryst. Solids **107**, 187 (1989).
[38]N. Lebedev, Proc. State Opt. Inst. Leningr. **2**, 10 (1921).
[39]N. Valenkov and E. A. Porai-Koshits, Z. Kristallogr. A **95**, 195 (1936); E. A. Porai-Koshits, J. Non-Cryst. Solids **73**, 79 (1985).
[40]W. H. Zachariasen, J. Am. Chem. Soc. **54**, 3841 (1932).
[41]J. C. Phillips, in *Solid State Physics,* edited by H. Ehrenreich, F. Seitz, and D. Turnbull (Academic, New York, 1982), Vol. 37, p. 93; J. C. Phillips, Phys. Rev. B **32**, 5350 (1985).
[42]R. J. Bell and P. Dean, Nature (London) **212**, 1354 (1966); R. J. Bell and P. Dean, Philos. Mag. **25**, 1381 (1972).
[43]P. H. Gaskell and I. D. Tarrant, Philos Mag. B **42**, 265 (1980).
[44]J. L. Robertson and S. C. Moss, J. Non-Cryst. Solids **106**, 330 (1988).
[45]P. Keating, Phys. Rev. **145**, 637 (1966).
[46]P. N. Sen and M. F. Thorpe, Phys. Rev. B **15**, 4030 (1977).
[47]M. F. Thorpe and F. L. Galeener, Phys. Rev. B **22**, 3078 (1980).
[48]S. W. de Leeuw and M. F. Thorpe. Phys. Rev. Lett. **55**, 2879 (1985); M. F. Thorpe and S. W. de Leeuw, Phys. Rev. B **33**, 8490 (1986).
[49]L. Guttman and S. M. Rahman, Phys. Rev. B **16**, 2942 (1988).
[50]R. B. Laughlin and J. D. Joannopoulos, Phys. Rev. B **16**, 2942 (1977).
[51]F. L. Galeener, R. A. Barrio, E. Martinez, and R. J. Elliott, Phys. Rev. Lett. **53**, 2429 (1984).
[52]R. A. Barrio, F. L. Galeener, and E. Martinez, Phys. Rev. Lett. **52**, 1786 (1984).
[53]A. Rahman, R. H. Fowler, and A. H. Narten, J. Chem. Phys. **57**, 3010 (1972).
[54]L. V. Woodcock, C. A. Angell, and P. Cheeseman, J. Chem. Phys. **65**, 1565 (1976).
[55]T. F. Soules, J. Chem. Phys. **71**, 4570 (1979); T. F. Soules, J. Non-Cryst. Solids **49**, 29 (1982).
[56]S. K. Mitra, M. Amin, F. Fincham, and R. W. Hockney, Philos. Mag. B **43**, 365 (1981).
[57]S. K. Mitra, Philos. Mag. B **45**, 529 (1982).
[58]S. H. Garofalini, J. Chem. Phys. **76**, 3189 (1982).
[59]J. D. Kubicki and A. C. Lasaga, Am. Mineral. **73**, 941 (1988).
[60]B. Feuston and S. H. Garofalini, J. Chem. Phys. **89**, 5818 (1988).
[61]F. H. Stillinger and T. A. Weber, Phys. Rev. B **31**, 5262 (1985).
[62]A. J. Dekker, *Solid State Physics* (Prentice-Hall, Englewood Cliffs, 1957), p. 127.
[63]J. P. Rino, Y. M. M. Hornos, G. A. Antonio, I. Ebbsjö, R. K. Kalia, and P. Vashishta, J. Chem. Phys. **89**, 7542 (1988); P. Vashista, I. Ebbsjö, R. Dejus, and K. Sköld, J. Phys. C **18**, L291 (1985); P. Vashishta and A. Rahman, Phys. Rev. Lett. **40**, 1337 (1978); J. Ray and P. Vashishta, J. Chem. Phys. **90**, 6580 (1989).
[64]P. Vashishta, R. K. Kalia, and I. Ebbsjö, Phys. Rev. B **39**, 6034 (1989); H. Iyetomi, P. Vashishta, and R. K. Kalia, J. Phys. Condens. Matter **1**, 2103 (1989).
[65]P. Vashishta, R. K. Kalia, G. A. Antonio, and I. Ebbsjö, Phys. Rev. Lett. **62**, 1651 (1989).
[66]C. Kittel, *Introduction to Solid State Physics,* 4th ed. (Wiley, New York, 1971).
[67]D. Beeman and R. Alben, Adv. Phys. **26**, 339 (1977).
[68]G. A. Antonio, B. P. Feuston, R. K. Kalia, and P. Vashishta, J. Chem. Phys. **88**, 7671 (1988); B. P. Feuston, R. K. Kalia, and P. Vashishta, Phys. Rev. B **35**, 6222 (1987).
[69]R. Fletcher, *Practical Methods of Optimization* (Wiley, New York, 1980).
[70]S. Susman, D. L. Price, K. J. Volin, and R. J. Dejus, J. Non-Cryst. Solids **106**, 26 (1988).
[71]A. C. Wright and C. N. J. Wagner, J. Non-Cryst. Solids **106**, 85 (1988).
[72]L. A. Curtis (private communication).

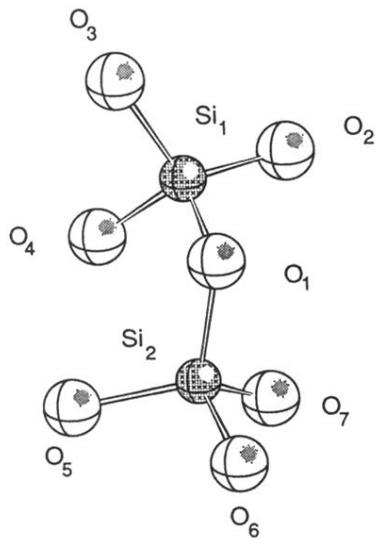

FIG. 9. A schematic view of corner-sharing tetrahedra in *a*-SiO_2.